PCCP

Accepted Manuscript




ROYAL SOCIETY OF CHEMISTRY

www.rsc.org/pccp

Physical Chemistry Chemical Physics RSCPublishing

ARTICLE

# Adhesion force interactions between cyclopentane hydrate and physically and chemically modified surfaces

Cite this: DOI: 10.1039/x0xx00000x

Received 00th January 2012,
Accepted 00th January 2012

DOI: 10.1039/x0xx00000x

www.rsc.org/

Zachary M. Aman,[a*] E. Dendy Sloan,[b] Amadeu K. Sum,[b] Carolyn A. Koh[b*]

Interfacial interactions between liquid-solid and solid-solid phases/surfaces are of fundamental importance to the formation of hydrate deposits in oil and gas pipelines. This work establishes the effect of five categories of physical and chemical modification to steel on clathrate hydrate adhesive force: oleamide, graphite, citric acid ester, nonanedithiol, and Rain-X anti-wetting agent. Hydrate adhesive forces were measured using a micromechanical force apparatus, under both dry and water-wet surface conditions. The results show that the graphite coating reduced hydrate-steel adhesion force by 79%, due to an increase in the water wetting angle from 42±8° to 154±7°. Two chemical surface coatings (nonanedithiol and the citric acid ester) induced rapid hydrate growth in the hydrate particles; nonanedithiol increased hydrate adhesive force by 49% from the baseline, while the citric acid ester coating reduced hydrate adhesion force by 98%. This result suggests that crystal growth may enable a strong adhesive pathway between hydrate and other crystalline structures, however this effect may be negated in cases where water-hydrocarbon interfacial tension is minimised. When a liquid water droplet was placed on the modified steel surfaces, the graphite and citric acid ester became less effective at reducing adhesive force. In pipelines containing a free water phase wetting the steel surface, chemical or physical surface modifications alone may be insufficient to eliminate hydrate deposition risk. In further tests, the citric acid ester reduced hydrate cohesive forces by 50%, suggesting mild activity as a hybrid anti-agglomerant suppressing both hydrate deposition and particle agglomeration. These results demonstrate a new capability to develop polyfunctional surfactants, which simultaneously limit the capability for hydrate particles to aggregate and deposit on the pipeline wall.

## Introduction

Gas hydrates are solid inclusion compounds, where molecular cages of water surround small hydrocarbon species at high pressure and low temperature.[1] In oil and gas transportation, hydrate may form as oil- or gas-dominant process fluids exchange heat with seawater leading to complete pipeline blockage. The present work focuses on hydrate blockage risk in early- to mid-life oil systems, which may be characterised by a low to moderate water fraction emulsified/dispersed in a bulk oil phase. In such systems, liquid water may be partially or fully dispersed in the liquid hydrocarbon phase, enabling hydrate formation at the oil-water interface.[2] Turner et al.[3] proposed that the initial growth of a hydrate film across the oil-water interface is limited to approximately 100 μm. That is, dispersed water droplets with radii less than 50 μm may convert to solid particles during the initial hydrate growth period, while larger droplets may retain a liquid water core that shrinks with time.[4] The dispersion of solid particles in oil has been observed to increase the effective viscosity of the liquid phase[5, 6] and, by extension, the pressure drop required to maintain a given flowrate.[7] Yang et al.[8] presented the first measurements of strong cohesive force between hydrate particles (tetrahydrofuran), which may be generally characterised as a granulation-type phenomenon.[9] Sinquin et al.[6] inferred that strong interparticle interactions may result in fractal hydrate aggregates[10, 11] that further increase slurry viscosity. Recent studies have suggested a jamming-type failure mechanism,[12] where large hydrate/particle aggregates[13] may fully occlude flow in the pipeline.

The avoidance of hydrate plug formation is currently achieved by either (i) removing the system from hydrate forming conditions in terms of pressure and temperature, or (ii) injecting hydrate surface active chemicals that interfere with hydrate agglomeration tendancy. The latter class, low dosage hydrate inhibitors (LDHIs), are discussed in detail by Kelland,[14] and include hydrate anti-agglomerants (AAs). AAs are typically ionic surfactants that, as a possible mechanism, adsorb to the hydrate-oil interface, effectively creating hydrophobic hydrate

surfaces that minimise hydrate cohesive force. To date, AAs have not been validated for use in reducing hydrate film growth or deposition on the pipeline wall, which represents a critical failure mechanism in mid- to late-term hydrate plug formation with oil systems.[15] The hydrate-steel adhesive forces discussed in this study are also critical to describing the formation of hydrate deposits on the pipeline wall. While the preliminary studies described below have provided order-of-magnitude estimates for hydrate adhesive force, this study introduces the first experimental evidence of surface coatings that may be used to simultaneously control hydrate agglomeration and deposition on the pipeline wall.

Joshi et al.[16] measured pressure drop hysteresis during hydrate plug formation and dissociation in a four-inch flowloop, where heating from the pipeline wall may have dislodged hydrate deposits that grew during the later stages of hydrate plug formation. Substantial effort has been expended to quantify hydrate formation and growth in oil and water phases, however the mechanisms behind hydrate deposition, and its affect on the formation of a complete hydrate blockage, remain largely unknown. Hydrate film growth on, and particle adhesion[17] to, the pipeline wall have been discussed in literature as potential mechanisms[18] to support the formation and growth of a hydrate deposit. Aman et al.[19] presented a hydrate interparticle force model with fundamental input of interfacial properties, including hydrate growth rate and the interfacial tension between hydrate-oil,[20, 21] hydrate-water and water-oil phases; surfactants may be used to manipulate these interfacial tension values, to exert a fundamental control on hydrate plug formation. Nicholas et al.[22] flowed water-saturated condensate in a single-pass flowloop under hydrate-forming conditions, measuring uniform pressure drop increases (<70 mbar/hr) with water fractions at or below the saturation limit in condensate. This pressure drop behaviour was hypothesized to be the result of growing a hydrate film on the cool pipeline wall, where dissolved water may allow for the slow growth and thickening of the deposit. Rao et al.[23] provided the first visual confirmation of hydrate film growth by flowing water-saturated methane over a cold surface in a single-pass configuration. Both Nicholas et al.[22] and Rao et al.[23] reported that the hydrate film increased heat transfer resistance in the system, with the latter study estimating a decrease in film porosity from 80 to 0% over a 60-hour period. The heat transfer limitations observed in both studies suggest that additional mechanisms, such as hydrate particle deposition from the liquid slurry, may contribute toward the formation of a complete hydrate blockage in the pipeline.

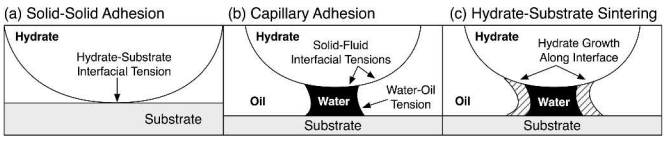


Figure 1. Mechanisms of hydrate-substrate adhesion adapted from Aman et al.:[19] (a) solid-solid adhesion force is governed by the product of interfacial area created by separation and solid-fluid interfacial tension; (b) capillary adhesion force is governed by the strength of the water bridge connecting both solids, which is a function of the three noted interfacial tensions; and (c) sintering adhesion force is a function of both the size of the growing hydrate bridge and hydrate tensile strength.

As a first approximation, adhesive interactions between hydrate particles and substrates may be extended from three fundamental hydrate cohesive mechanisms discussed by Rabinovich et al.[24, 25] and Aman et al.[19] (shown in Figure 1). Solid-solid adhesion is the dominant mechanism in water-continuous systems,[26] while capillary adhesion[27, 28] is the dominant mechanism in oil-continuous systems, with a liquid water bridge[29, 30] binding hydrate particles together. Hydrate growth or sintering[31, 32] is a third ad/cohesive force mechanism in both water and oil phases, pending the availability of reactants at the contact point. Rabinovich et al.[24] demonstrated that the capillary force of adhesion between a particle and substrate may follow the same geometric principles as the cohesive (particle-particle) force, with the addition of the substrate's energetic contribution to the capillary bridge.

As discussed by Aman et al.,[19] the capillary cohesive or adhesive force ($F_A$) is described by equation 1:

$$\frac{F_A}{R^*} = \pi\gamma\sin(\alpha)\sin(\theta_p + \alpha) + \frac{2\pi\gamma\cos(\theta_p)}{1 + H/2d} \quad (1)$$

where $R^*$ is the radius of the particle (or particle pair, when applicable), $\gamma$ is the interfacial tension between water and oil, $\theta_p$ is the wetting angle of water on the hydrate and substrate surfaces, and $\alpha$ describes the maximum embracing angle of the water bridge on the hydrate surface with height $H$ and immersion depth $d$. The surface coatings deployed are all expected to increase the wetting angle of the steel surface ($\theta_p$) toward an oil-wetting condition, thereby reducing adhesive force. Surface coatings that are surfactant-based may duly reduce the interfacial tension between water and oil ($\gamma$), providing a further reduction in measured adhesive force. As an example calculation of eq (1) provided by Aman et al.,[19] a normalised cohesive force of 4.3 mN/m is obtained for cyclopentane hydrate in liquid cyclopentane, where interfacial tension ($\gamma$) is approximately 51 mN/m, the water wetting angle ($\theta_p$) is 29°, with a 50 nm water layer ($H$) that results in embracing angle ($\alpha$) of 0.1° and immersion depth ($d$) of 0.7 nm.

Nicholas et al.[33] used a micromechanical force (MMF) apparatus to measure the adhesive force between cyclopentane hydrate particles on stainless steel, concluding pipeline shear stresses were sufficient to disrupt hydrate adhesion to dry pipeline walls (i.e. without a water layer). Aspenes et al.[34] extended these MMF measurements to water-wetted steel, concluding the presence of a capillary bridge increased hydrate adhesive force by a factor of 50×. When the bulk cyclopentane phase contained 0.6 wt% of naphthenic acid,[35-37] Aspenes et al.[34] measured a 50% decrease in this wetted adhesive force. These experiments suggest that the surface wetting condition may represent a critical risk to hydrate particle deposition.[18]

The present investigation builds upon the work above by measuring cyclopentane hydrate adhesive force with a series of chemically and physically modified stainless steel surfaces, to identify conditions that minimize the hydrate-solid adhesion interactions, and hence risk of hydrate deposition. The combination of reducing adhesion and cohesion interactions is also examined for the most effective chemically modified substrate. The work deploys a MMF apparatus with short contact durations in preference to static adhesion methods



 

reported in the literature,[38] which focus attention on the strength of fully-sintered hydrate.

## Experimental Methods

### Micromechanical Force Measurements

The MMF apparatus consisted of an inverted light microscope (Zeiss Axiovert Observer), with an experimental cell (internal volume of 10 ml) placed on the microscope stage (Figure 2). The cell consisted of an aluminium dish with a transparent glass centrepiece to allow the microscope light path through experimental fluids. The cell was outfitted with a glycol-water cooling jacket with a temperature range of -5 to 20 °C and a precision of ±0.1 °C. Hydrate particles were placed on the tips of calibrated glass cantilevers with 35 μm external diameter, which were secured inside capillary holders and attached to an external micromanipulation system. The left-hand cantilever (Figure 2) was controlled by a manual micromanipulator, while the right-hand cantilever position was controlled with a remotely-operated Eppendorf Patchman micromanipulator (1 μm precision). The microscope and micromanipulators were placed in a dry box filled with cyclopentane-saturated nitrogen gas, atop an active pneumatic vibration isolation table. A comprehensive description of the MMF design and operation apparatus is provided in the literature.[19]

To generate the hydrate particle, a droplet of deionized water (500-1000 μm diameter) was placed on the tip of the glass cantilever. This droplet was quenched in liquid nitrogen to form ice, and was placed in the experimental cell, which was filled with liquid cyclopentane (99%; Sigma-Aldrich) maintained at -5 °C. The cell temperature was then raised to 3.2 °C over the course of 30 minutes. The melting ice provided a consistent growth pathway for a cyclopentane hydrate. Previous experiments using this hydrate formation technique[19] have demonstrated that a thin cyclopentane hydrate shell (50-100 μm) forms at the water-cyclopentane interface, while the particle interior remains liquid water due to mass transfer limitations across the shell. The hydrate shell was annealed for one hour before beginning the experiment.

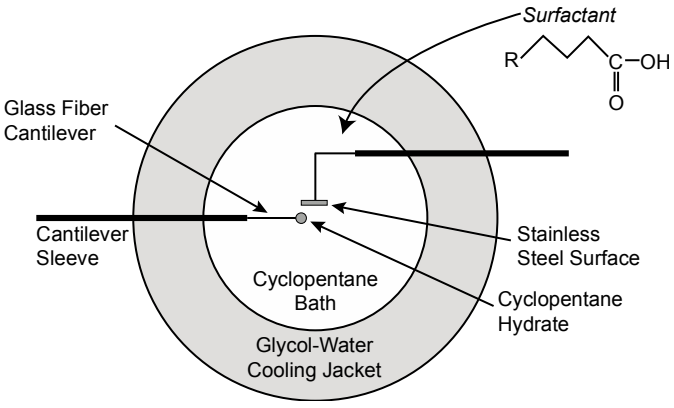


Figure 2. (left) Schematic of the experimental cell from above, where a substrate is brought into contact with a cyclopentane hydrate particle, adapted from Aman et al.[19]

In each adhesive force trial, 40 pull-off measurements were performed according to the four-step procedure in Figure 3. Aman et al.[39] established the reproducibility of MMF measurements through a systematic study of cohesive force, establishing the use of normal error bounds to describe confidence in the average pull-off value obtained. The maximum displacement in each pull-off ($\Delta_D$ in Figure 3) was multiplied by the spring constant of the bottom cantilever, to obtain the adhesive force (i.e. deploying Hooke's law). The final adhesive force is reported as the average of all pull-off trials from three independent experiments (with 40 pull-off trials each).

To confirm the repeatability of these measurements, two independent hydrate adhesion tests were performed with different oleamide-coated substrates and calibration constants; the average force values were within agreement at 95% confidence (0.34 ± 0.29 mN/m, and 0.39 ± 0.07 mN/m). These pull-off steps were also deployed to study hydrate cohesion force, by replacing the top substrate with a second hydrate particle. Only one hydrate-steel contact point was used in each experiment, which was identified from the visually smoothest point of both surfaces.

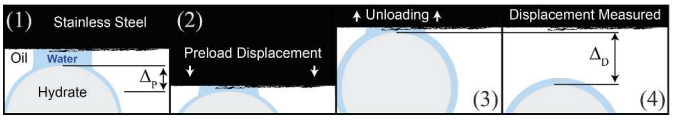


Figure 3. Experimental steps in pull-off measurement of hydrate adhesion, where the substrate is moved from a resting position (step 1) to apply a pre-load displacement ($\Delta_p$ in step 2). After a 10-second contact time, the substrate is raised (step 3) to a maximum displacement ($\Delta_D$) which is captured visually (step 4).

Cyclopentane hydrate adhesive force was measured for each stainless steel wafer *before* any chemical or physical modification was applied, to establish a baseline force for comparison with Aspenes et al.[34] The ratio between the baseline force of each steel wafer and the established average[34] was then used to linearly scale all data collected with the wafer (at the same particle-steel contact point) after the chemical/physical coating was applied. This calibration technique was also deployed by Aman et al.[40] to ensure consistency between cohesive force measurements, which accounted for variable surface roughness (hydrate and substrate) and water saturation in the liquid cyclopentane bulk phase.

### Surface Coatings

Stainless steel (grade 309) was selected as the baseline surface, based on an established hydrate adhesive force of 0.83±0.12 mN/m.[34] Square wafers of steel (1 $cm^2$) were cleaned according to a three-step procedure: (i) steel surfaces were rinsed for 10 seconds with a Sodosil alkaline solution (10 vol% in water); (ii) the steel was then rinsed for 60 seconds with high-purity ethanol; and (iii) the steel was finally rinsed for 60 seconds in acetone. After this rinsing procedure, the wafers were placed in a sealed container for storage to minimize contact with the environment. Five surface modifications were selected: (i) oleamide $(CH_3)(CH_2)_8(CH)_2(CH_2)_7CONH_2$; (ii) a citric acid ester, based on $HOC(COOH)(CH_2COOH)_2$; (iii) nonanedithiol $HSCH_2(CH_2)_7CH_2SH$; (iv) commercial Rain-X®; and (v) graphite, based on planar sheets of carbon. These surface

coatings were chosen as representatives of three functional categories, with a goal of establishing a basis for whether surface modifications could ultimately be used to simultaneously control hydrate agglomeration and deposition phenomena. Oleamide, citric acid ester, and nonanedithiol were selected based on studies by Aman et al.,[41] which demonstrated the importance of a surfactant hydrophilic head in reducing hydrate interparticle force. These three chemistries each provide a functional aliphatic hydrophobic group, while respectively testing the effectiveness of carbon (carboxyl), nitrogen (amide), and sulphur (thiol) hydrophilic head groups. Commercial Rain-X was added to this list as a comparison against a commercial agent used to modify substrate hydrophilicity. Similarly, graphite was chosen to enable direct comparison of the functional chemistries with a strong hydrophobic surface; the practical requirements of continuously injecting graphite in flowlines to combat erosion would preclude its use. The first four modifications were chemical in nature, where each stainless steel wafer was submerged in the liquid chemical (at room temperature) for five seconds, removed, and placed in a dry environment for at least 24 hours prior to use. The fifth modification was physical, where the steel surface was etched with a graphite sample until visibly darker; excess graphite was removed by gently passing a paper towel over the surface. Multiple modified steel wafers were prepared with each modification, and were removed from use after each experiment.

**Contact Angle and Interfacial Tension**

The static wetting angle of deionized water (sessile drop) on stainless steel surfaces was measured visually on an interfacial tensiometer (KSV Instruments) at room temperature and ambient pressure. Wetting angle data were only used qualitatively in select experiments, to aid in interpreting MMF adhesive force data. With select chemical modifications, varying fractions of surfactant were mixed in the mineral oil phase at 60 °C until it was visibly homogeneous; further details on the mineral oil and a detailed measurement procedure are provided in Aman et al.[40] In each wetting angle experiment, a deionised water droplet (~ 20 microliters in volume) was placed atop the coated surface with a Hamilton gastight syringe in the presence of air; images of the droplet were recorded from a precision stand (KSV surface tensiometer instrument), mounted directly in front of the droplet. The wetting angle was measured until it achieved a steady-state value; the reported wetting angle represents an average of at least six independent experiments, with 95% confidence boundaries. The interfacial tension between a droplet of deionized water in modified mineral oil was measured visually (pendant drop) on an interfacial tensiometer (KSV Instruments) with one-second recording interval that started immediately after creating the water droplet.

Results and DiscussionHydrate adhesive forces were measured for each chemically or physically modified stainless steel surface, with three independent experiments for each. Rain-X®, graphite and oleamide modifications were tested with 40 pull-off trials per experiment (120 pull-off trials total), however the nonanedithiol and citric acid ester modifications were tested over a total of 42 and 80 pull-off trials, respectively, due to both chemicals resulting in hydrate morphological changes (discussed below). Each surface modification was observed to change the average hydrate adhesive force from the established baseline (Figure 4). Average adhesive force on Rain-X® and oleamide surfaces decreased by 32 and 33% from the baseline (plain steel),[34] respectively, which is within one standard deviation of the plain steel force. Contact between the hydrate and nonanedithiol surface resulted in a 49% *increase* in hydrate adhesive force, due to significant hydrate growth observed at the particle-steel contact point (discussed below). The lowest adhesive forces were obtained with the graphite and citric acid ester surfaces, respectively 79 and 98% below the plain steel baseline.

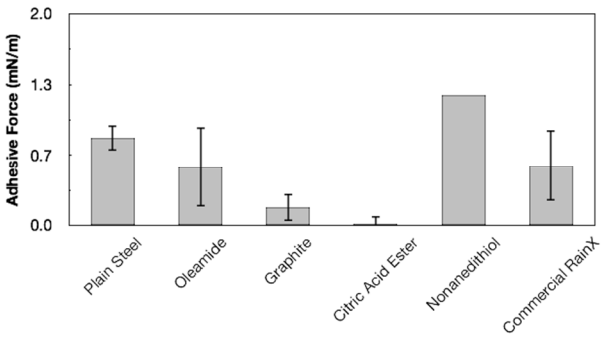


Figure 4. Cyclopentane hydrate adhesive force measurements for untreated and physically/chemically modified stainless steel surfaces; error bounds represent one standard deviation of 40-120 pull-off measurements.

An example of the hydrate growth observed with nonanedithiol is shown in Figure 5, where a cylindrical hydrate feature grew at the particle-substrate contact point. The growth of this feature was observed in three independent experiments, and began immediately after contact with the particle, and increased hydrate adhesive force as per Figure 4. In the third experiment (bottom row of Figure 5), the adhesive force between the cylindrical hydrate growth and nonanedithiol-coated steel was sufficiently large to result in fracture at the particle-feature interface. Chemical additives[42, 43] and subcooling from equilibrium[44] have been previously observed to affect hydrate morphology; as demonstrated by Aman et al.,[19] this hydrate growth behaviour may be the result of liquid water migrating from the particle core to the surface.

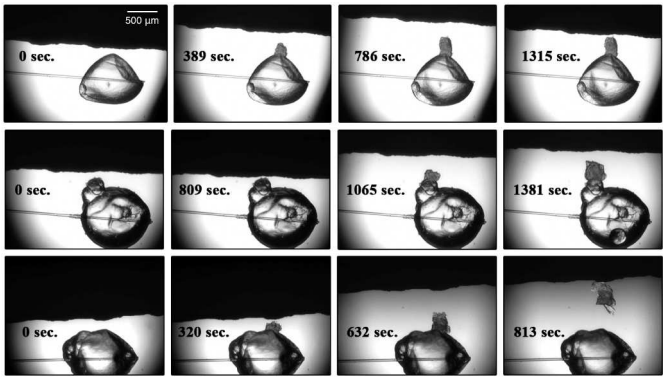


Figure 5. Three examples (each row) of hydrate growth and morphology change during contact with nonanedithiol-coated surface, where a cylindrical hydrate feature was observed to grow at the hydrate-steel contact point over time.

For the stainless steel coated with the citric acid ester, hydrate morphology was observed to change immediately after the hydrate particles were *exposed* to the steel surface. For both trials shown in Figure 6, hydrate morphology changed within 30 seconds of introducing the substrate to the experimental cell, and occurred *before* the substrate had contacted the hydrate particle. This behaviour may suggest that the citric acid ester diffused through the liquid cyclopentane to reach the hydrate particle surface; diffusion through the liquid phase may have been accelerated due to turbulence in the liquid generated by inserting the substrate. After 60 seconds of exposure (top row, Figure 6) droplets of liquid cyclopentane were observed inside the hydrate particle core; within 100 seconds, the hydrate particle began growing beyond the original hydrate shell. Over the course of the experiment, the particle shade consistently changed from light to dark, which may be the result of enhanced hydrate conversion. Hydrate growth of this kind, where liquid cyclopentane droplets were observed to form inside the hydrate shell, is similar to observations from Aman et al.[19] when cyclopentane hydrate was exposed to alkyl benzene sulfonic acid. Similar to nonanedithiol measurements, the specific mechanism behind how chemical additives interact with the hydrate interface to encourage growth is not well understood and is an on-going subject of investigation. One possible hypothesis to explain why the citric acid ester both decreased adhesive force *and* encouraged hydrate growth is that the citric acid ester is a much stronger surfactant than nonanedithiol (discussed further below), which may substantially weaken the hydrate-steel capillary bridge (Figure 1).[19] In sufficient quantity, a strong surfactant may reduce the interfacial energy barrier to growth, enabling the rapid morphological changes observed in Figure 6.

Recent studies from Lo et al.[45, 46] and Zhang et al.[47] have investigated the dependence of zeta potential of hydrate slurries on the concentration of surfactant (e.g. sodium dodecyl sulphate) in the liquid phase, extracting estimates on the amount of surfactant adsorbed to the hydrate. Aman et al.[40] similarly deployed both interfacial tensiometry and micromechanical force measurements to estimate the dependence of hydrate-oil interfacial tension on surfactant concentration. These methods may be used to identify the respective hydro- and hydrate-philicity for morphology-changing chemical additives (e.g., nonanedithiol), and to provide insight as to where the additive will adsorb in a multiphase system.

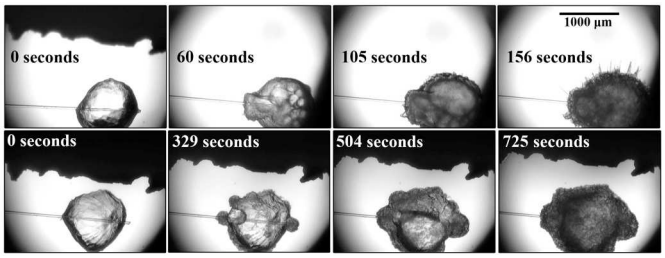


Figure 6. Two examples (each row) of hydrate growth and morphology change during contact with a citric acid ester-coated stainless steel surface.

**Effect of Water on Adhesive Force**

As discussed above, the severity of hydrate deposition on pipeline walls may be linked to the wetting condition of the wall.[18] To study this condition, adhesion forces were measured for the plain, graphite-coated, and citric acid ester-coated stainless steel during water-wet conditions. To first probe this effect, a small droplet (approximately 200 µm diameter) of deionized water was placed on the substrate surface with a pipette; the hydrate particle was contacted directly with this droplet during stages 2 and 3 of the pull-off trial (Figure 3). As the substrate surface was raised, a large water bridge (200 µm diameter) was observed visually; the eventual rupture of this bridge resulted in a small fraction of water partitioning to the hydrate particle, corresponding to the "wet particle, wet surface" condition in the middle pane of Figure 8. Four pull-off trials were performed for each surface in this wet condition, and the average forces are provided in Figure 8. For reference, the static wetting angles of deionized water (in a bulk phase of air) on each surface are also provided for reference, with error bounds representing 95% confidence intervals over six repeat trials. After these four trials, an additional 40 pull-off trials were performed where the wetted hydrate particle (i.e. the hydrate particle retained an unconverted water layer after contacting the deionised water droplet) was contacted with a "dry" position on the substrate surface (i.e. a minimum of 5000 µm away from the water droplet position). An example experimental image of the "wet particle, dry surface" conditions is shown in Figure 7 with the data reported in the right-hand pane of Figure 8, and provide a qualitative indication of how effectively the surface will repel a capillary bridge from the hydrate particle.

The results in Figure 8 demonstrate that the presence of a water droplet on each surface increased hydrate adhesive forces by a factor of 50 (plain steel) to 500 (citric acid ester). The wetting angle of water on the steel surface did not strongly affect these wetted adhesion forces, which strictly represents only a non-flowing condition within the pipeline. The effect of surface wettability is seen more clearly in the right-hand pane of Figure 8, where adhesive forces on the graphite-coated surface is similar for dry and water-wet hydrate particles. Contact between the wet hydrate particle and citric acid ester-coated surfaces results in a larger adhesive force, approximately 10× that of the dry hydrate particle. All pull-off trials corresponding to dry and water-wet hydrate (with the citric acid ester-coated surface) are plotted in Figure 9, for two independent experiments.

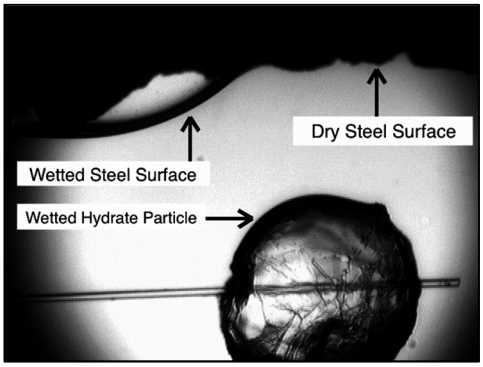


Figure 7. Example of wetted hydrate adhesion force tests, where the hydrate particle is first contacted with a water droplet to generate a wetted hydrate condition, and adhesion forces are subsequently measured with a dry steel surface. The continuous fluid is high-purity liquid cyclopentane in all experiments.

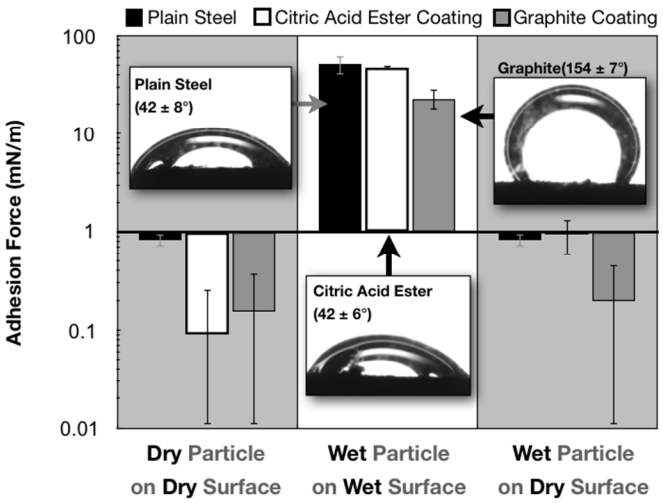


Figure 8. Cyclopentane hydrate adhesive force on uncoated (baseline condition), graphite-coated and citric acid ester-coated stainless steel under three wetting conditions (as illustrated in Figure 7). A visual key is given for the wetting condition in each stage:
*(1) a dry hydrate particle contacting a clean steel surface, shown in the left panel;*
*(2) a hydrate particle contacting a water droplet on the steel surface, shown in the middle panel; and*
*(3) a water-coated hydrate particle contacting a clean steel surface, shown in the right panel.*
The experimental images report average wetting angle, and correspond only to the middle panel condition with a wet surface. Error bounds represent one standard deviation of all data collected.

The results demonstrate that, prior to wetting the hydrate particle with water, no trend is observed in the pull-off trials. Immediately after the wetting period (i.e. contact with a water droplet on the substrate surface), hydrate adhesion forces increased by a factor of 10-25×. During the first 20 pull-off trials after the water wetting period (i.e. pull-offs 45-64 in Figure 9), hydrate adhesive forces were observed to decrease to a steady-state value that was approximately 10× larger than the average force *prior* to contact with the water droplet. The introduction of a water droplet means the system will not be at chemical equilibrium, however the force measurements are resolved through only a requirement of mechanical stability. The goal of these measurements is to resolve the temporal effect of the reacting water droplet on the ultimate hydrate cohesive force (Figure 9).

The data presented in Figure 8 suggest two important consequences of water-coated pipeline walls on hydrate adhesion force and deposition potential. First, control of the pipeline wettability may be insufficient to prevent hydrate adhesion during periods with minimal (or without) flow; the formation of a liquid water phase at the oil-pipeline boundary may increase the hydrate adhesive force by 2-3 orders of magnitude. Second, exposing hydrate particles to a liquid water phase may irreversibly affect the hydrate adhesive force (within the residence time of the pipeline); each experiment presented in Figure 9 required approximately 90 minutes of experimental time. This understanding may be critical in considering hydrate control during restart operations, where liquid water has segregated and wetted the pipeline wall.

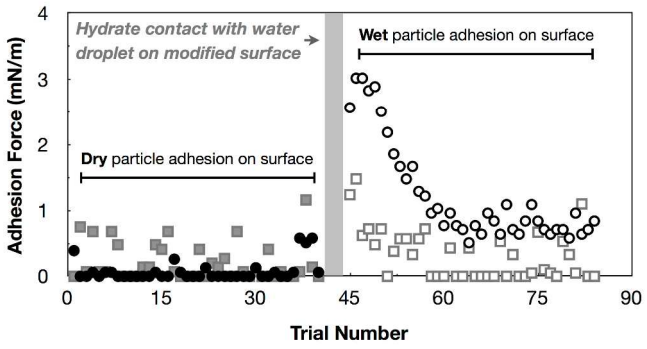


Figure 9. Hydrate adhesive forces on citric acid ester-coated steel over two experiments (● and ■) under two wetting conditions: dry particle on dry surface (pull-off trials 0-40), and wet particle on dry surface (pull-off trials 45-84).

**Citric Acid Ester Effect on Cohesive Force**

The citric acid ester surface modification reduced hydrate adhesive force by 98% under dry conditions (Figure 4) while the chemical demonstrated excellent solubility in the liquid cyclopentane phase. This data raised a natural question of whether the citric acid ester may be suitable to use as a hydrate anti-agglomerant,[14, 48] by reducing the aggregation force between hydrate particles, in addition to reducing surface-particle interactions. To probe this question, water-oil interfacial tension (IFT) and hydrate interparticle cohesive force were measured with varying concentrations of citric acid ester in the liquid hydrocarbon phase.

At the lowest concentration tested (250 ppm by mass), the citric acid ester significantly reduced the IFT between deionized water and mineral oil from a baseline of 55 mN/m (Figure 10-A). The initial and steady-state (final) IFT values decreased monotonically with increasing concentration of citric acid ester in the mineral oil (through 1000 ppm). The water droplets could be only captured for a limited amount of time, as the IFT values decreased to a point that droplets were no longer stable on the syringe tip (approaching a limiting capability of this method);[40] this limitation prevented the measurements from reaching steady-state in the 750 and 1000 ppm systems (Figure 10-A).

The average steady-state IFT values are plotted in Figure 10-B as a function of citric acid ester concentration for six independent trials, alongside hydrate cohesive force measurements (in a liquid cyclopentane bulk phase) over a similar mass fraction range. With a baseline (0 ppm) IFT value of 55 mN/m, the data in Figure 10-B demonstrate that decreases in both IFT and cohesive forces are not proportional. That is, the addition of 200 ppm citric acid ester decreases water-oil IFT by 85%, while the same amount of acid decreases hydrate cohesive force by approximately 50%. This comparison qualitatively suggests that the citric acid ester may exhibit higher affinity for water-oil than hydrate-oil interfaces; this hypothesis may be further explored by measuring adsorption isotherms per the above-described methods.[40, 45-47]

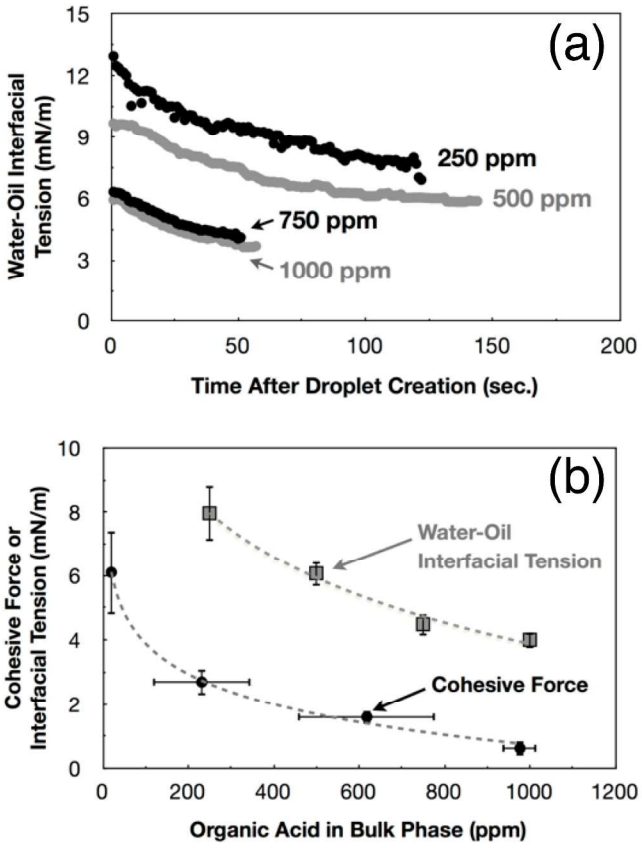


Figure 10. (A) dynamic interfacial tension between deionized water and mineral oil containing 250-1000 ppm (by mass) of the citric acid ester additive; (B) steady-state interfacial tension (■) and hydrate interparticle cohesive force (●) as a function of citric acid ester fraction in the bulk phase (by mass); ordinate error bounds correspond to 95% confidence intervals, while abscissa error bounds represent the range of mass fractions tested. Dashed curves are provided to guide the eye.

Both datasets in Figure 10-B suggest that the effect of citric acid ester reaches an asymptotic value close to 1000 ppm, after which the cohesive force and interfacial tension may not substantially decrease with the addition of citric acid ester. While the acid decreased hydrate *adhesive* force by 98%, the chemical was not determined to be as effective at reducing hydrate cohesive force compared with previous studies by Aman et al.[40] with various surfactant types.

The application of this insight requires validation in a high-pressure micromechanical force apparatus, to compare the cohesive and adhesive behaviour of cyclopentane and natural gas hydrate. The performance of anti-agglomeration and deposition coatings may be scaled using a high-pressure flowloop apparatus in the future.

## Conclusions

Using a micromechanical force (MMF) method, hydrate-steel adhesive forces were tested with five different chemical or physical modifications, with the goal of identifying methods to reduce hydrate particle deposition on the wall of oil and gas pipelines. The addition of graphite on the steel surface reduced adhesion force by 79% compared to plain stainless steel, which may be due to a change in the water wetting angle on steel: 154±7° with graphite-coated steel, and 42±8° for plain steel. Coating the stainless steel with a citric acid ester decreased baseline adhesive force by 98% and resulted in severe morphology changes that accelerated growth in the hydrate particle; these morphology changes did not increase the hydrate adhesive force, as adsorption of the citric acid ester surfactant will decrease water-oil interfacial tension and, by extension, the hydrate-steel capillary bridge. Hydrate contact with nonanedithiol-coated surfaces resulted in a different class of morphological growth, where a cylindrical hydrate feature formed at the particle-surface contact point that increased adhesive force by 49% from the baseline.

The effectiveness of citric acid ester and graphite coatings decreased when a droplet of deionized water was placed on the substrate surface; the coatings reduced average adhesive force by 7 and 55%, respectively, with water-wetted surfaces. Hydrate particle contact with a liquid water phase irreversibly increased hydrate-steel adhesive forces, which were approximately 10× larger than trials with a dry hydrate particle. Interfacial studies were deployed to identify why the citric acid ester reduced hydrate-steel adhesion force, which suggested qualitatively that the chemical may adsorb more readily to the hydrate-oil interface than the water-oil interface. That is, hydrate-philic chemical structures may preferentially order at periodic hydrogen bonding sites on the hydrate surface, which may be identified by changes to the adsorption isotherm for water-oil and hydrate-oil interfaces.[14]

## Acknowledgements

The authors acknowledge support from the Colorado School of Mines Hydrate Consortium (current and past members): BP, Chevron, ConocoPhillips, ENI, ExxonMobil, Halliburton, MultiChem, Nalco, Petrobras, Schlumberger, Shell, SPT Group, Statoil and Total. C.A.K. acknowledges partial support by the U.S. Department of Energy, Office of Basic Energy Sciences, Division of Materials Sciences and Engineering (DOE-BES award DE-FG02-05ER46242).

## Contact Information

[a] Centre for Energy, Mechanical and Chemical Engineering, The University of Western Australia, 35 Stirling Highway, Crawley, AUSTRALIA.

[b] Center for Hydrate Research, Department of Chemical & Biological Engineering, Colorado School of Mines, Golden, USA.

* Corresponding authors: zachary.aman@uwa.edu.au, +61 6488 3078; ckoh@mines.edu, +1 303 273 3237

## References

1. E. D. Sloan and C. A. Koh, *Clathrate Hydrates of Natural Gases*, Third Edition edn., CRC Press, Taylor & Francis Group, Boca Raton, FL, 2007.
2. Y. Fan, S. b. Simon and J. Sjoblom, *Energy & Fuels*, 2009, **23**, 4575-4583.
3. D. Turner, K. Miller and E. Sloan, *Chemical Engineering Science*, 2009, **64**, 3996-4004.
4. A. S. Stoporev, A. Y. Manakov, L. K. Altunina, A. V. Bogoslovsky, L. A. Strelets and E. Y. Aladko, *Energy & Fuels*, 2014, **28**, 794-802.
5. J. Sjoblom, N. Aske, I. Auflem, O. Brandal, T. Havre, O. Saether, A. Westvik, E. Johnsen and H. Kallevik, *Advances in Colloid and Interface Science*, 2002, 399-473.
6. A. Sinquin, T. Palermo and Y. Peysson, *Oil & Gas Science and Technology*, 2004, **59**, 41-57.
7. H. Mukherjee and J. P. Brill, *International Journal of Multiphase Flow*, 1985, **11**, 299-315.
8. S.-o. Yang, D. Kleehammer, Z. Huo, J. Sloan, E Dendy and K. Miller, *Journal of Colloid and Interface Science*, 2004, **277**, 335-341.
9. J. Litster and B. Ennis, *The Science and Engineering of Granulation Processes*, Kluwer Academic Publishers, 2004.
10. H. Leba, A. Cameirao, J.-M. Herri, M. Darbouret, J.-L. Peytavy and P. Glenat, *Chemical Engineering Science*, 2010, **65**, 1185-1200.
11. M. Suzuki, Y. Muguruma, M. Hirota and T. Oshima, *Advanced Powder Technology*, 1990, **1**, 115-123.
12. P. G. Lafond, M. W. Gilmer, C. A. Koh, E. D. Sloan, D. T. Wu and A. K. Sum, *Phys. Rev. E*, 2013, **87**, 8.
13. A. A. Potanin, *Journal of Colloid and Interface Science*, 1991, **145**, 140-157.
14. M. Kelland, *Energy & Fuels*, 2006, **20**, 825-847.
15. G. A. Grasso, P. G. Lafond, Z. M. Aman, L. E. Zerpa, E. D. Sloan, C. A. Koh and A. K. Sum, 8th International Conference on Gas Hydrates, Beijing, China, 2014.
16. S. V. Joshi, G. A. Grasso, P. G. Lafond, I. Rao, E. Webb, L. E. Zerpa, E. D. Sloan, C. A. Koh and A. K. Sum, *Chemical Engineering Science*, 2013, **In Press.**
17. E. Bondarev, A. Groisman and A. Savvin, in *2nd International Conference on Natural Gas Hydrates*, Editon edn., 1996, pp. 95-99.
18. G. Aspenes, S. Hoiland, T. Barth, K. Askvik, R. Kini and R. Larsen, in *6th International Conference on Gas Hydrates (ICGH 2008)*, Editon edn., 2008.
19. Z. M. Aman, E. P. Brown, E. D. Sloan, A. K. Sum and C. A. Koh, *Physical Chemistry Chemical Physics*, 2011, 19796-19806.
20. D. Y. Kwok and A. W. Neumann, *Advances in Colloid and Interface Science*, 1999, **81**, 167-249.
21. D. Y. Kwok and A. W. Neumann, *Colloids and Surfaces A: Physicochemical and Engineering Aspects*, 2000, **161**, 31-48.
22. J. W. Nicholas, C. A. Koh, E. D. Sloan, L. Nuebling, H. He and B. Horn, *AIChE Journal*, 2009, **55**, 1882-1888.
23. I. Rao, C. A. Koh, E. D. Sloan and A. K. Sum, *Industrial & Engineering Chemistry Research*, 2013, **52**, 6262-6269.
24. Y. Rabinovich, M. Esayanur and B. Moudgil, *Langmuir*, 2005, **21**, 10992-10997.
25. Y. I. Rabinovich, M. S. Esayanur, K. D. Johanson, J. J. Adler and B. M. Moudgil, *Journal of Adhesion Science and Technology*, 2002, **16**, 1-18.
26. R. Asserson, A. Hoffmann, S. Hoiland and K. Asvik, *Journal of Petroleum Science and Engineering*, 2009, **68**, 209-217.
27. M. P. de Boer and P. C. T. de Boer, *Journal of Colloid and Interface Science*, 2007, **311**, 171-185.
28. H.-J. Butt and M. Kappl, *Advances in Colloid and Interface Science*, 2009, **146**, 48-60.
29. A. Doppenschmidt and H.-J. Butt, *Langmuir*, 2000, **16**, 6709-6714.
30. M. Bienfait, *Surface Science*, 1992, **272**, 1-9.
31. F. E. Kruis, K. A. Kusters, S. E. Pratsinis and B. Scarlett, *Aerosol Science and Technology*, 1993, **19**, 514-526.
32. T. Uchida, T. Shiga, M. Nagayama and K. Gohara, *Energies*, 2010, **3**, 1960-1971.
33. J. W. Nicholas, L. E. Dieker, E. D. Sloan and C. A. Koh, *Journal of Colloid and Interface Science*, 2009, **331**, 322-328.
34. G. Aspenes, L. E. Dieker, Z. M. Aman, S. Høiland, A. K. Sum, C. A. Koh and E. D. Sloan, *Journal of Colloid and Interface Science*, 2010, **343**, 529-536.
35. K. Erstad, S. Hoiland, T. Barth and P. Fotland, in *6th International Conference on Gas Hydrates (ICGH 2008)*, Editon edn., 2008.
36. A. Fafet, F. Kergall, M. Silva and F. Behar, *Organic Geochemistry*, 2008, **39**, 1235-1242.
37. T. Barth, S. Hoiland, P. Fotland, K. Askvik, B. Pedersen and A. Borgund, *Organic Geochemistry*, 2004, **35**, 1513-1525.
38. J. D. Smith, A. J. Meuler, H. L. Bralower, R. Venkatesan, S. Subramanian, R. E. Cohen, G. H. McKinley and K. K. Varanasi, *Physical Chemistry Chemical Physics*, 2012, **14**, 6013.
39. Z. M. Aman, S. E. Joshi, E. D. Sloan, A. K. Sum and C. A. Koh, *Journal of Colloid and Interface Science*, 2012, **376**, 283-288.
40. Z. M. Aman, K. Olcott, K. Pfeiffer, E. D. Sloan, A. K. Sum and C. A. Koh, *Langmuir*, 2013, **29**, 2676-2682.
41. Z. M. Aman, E. D. Sloan, A. K. Sum and C. A. Koh, *Energy & Fuels*, 2012, **26**, 5102-5108.
42. R. Sakemoto, H. Sakamoto, K. Shiraiwa, R. Ohmura and T. Uchida, *Crystal Growth & Design*, 2010, **10**, 1296-1300.
43. C.-Y. Sun, G.-J. Chen, C.-F. Ma, Q. Huang, H. Luo and Q.-p. Li, *Journal of Crystal Growth*, 2007, **306**, 1-9.
44. P. Servio and P. Englezos, *AIChE Journal*, 2003, **49**, 269-276.
45. C. Lo, J. Zhang, A. Couzis, P. Somasundaran and J. Lee, *J. Phys. Chem. C*, 2010, **114**, 13385-13389.
46. C. Lo, J. S. Zhang, P. Somasundaran, S. Lu, A. Couzis and J. W. Lee, *Langmuir*, 2008, **24**, 12723-12726.
47. J. Zhang, C. Lo, A. Couzis, P. Somasundaran, J. Wu and J. Lee, *J. Phys. Chem. C*, 2009, **113**, 17418-17420.
48. K.-L. Yan, C.-Y. Sun, J. Chen, L.-T. Chen, D.-J. Shen, B. Liu, M.-L. Jia, M. Niu, Y.-N. Lv, N. Li, Z.-Y. Song, S.-S. Niu and G.-J. Chen, *Chemical Engineering Science*, 2014, **106**, 99-108.